Journal of Food Engineering 88 (2008) 456–465

Contents lists available at ScienceDirect

Journal of Food Engineering

journal homepage: www.elsevier.com/locate/jfoodeng

Characterization of protein stabilized foam formed in a continuous shear mixing apparatus

Linda Indrawati, Ganesan Narsimhan *

Department of Agricultural and Biological Engineering, Purdue University, West Lafayette, IN 47907, United States

ARTICLE INFO

Article history:
Received 1 August 2007
Received in revised form 16 February 2008
Accepted 3 March 2008
Available online 18 March 2008

Keywords:
Protein stabilized foam
Foam formation
Bubble size
Syneresis
Liquid holdup profile
Apparent viscosity of foam
Sodium caseinate
Shear flow field
Air–liquid dispersion

ABSTRACT

A continuous shearing apparatus was employed to make sodium caseinate stabilized foams which was characterized by bubble size, apparent viscosity, foam volume fraction and liquid holdup profile. The bubble size of the foam was smaller for higher rotational speed of the rotor, lower ionic strength, pH away from p*I*, higher xanthan gum concentration and room temperature and did not vary significantly with air–liquid ratio. Bubble size at different gum concentrations correlated well with dimensionless Weber number. The foam volume fraction was higher at higher values of rotational speed, air–liquid ratio, xanthan gum concentrations and at pH 7 and 9. The evolution of liquid holdup profile indicated faster syneresis at higher ionic strength, higher temperature and lower air–liquid ratio. Collapse of the foam caused by syneresis was more pronounced at higher ionic strengths and higher temperature. The foam produced at pH 6 was drier with liquid holdup less than 0.26. The foam exhibited shear thinning behavior with the apparent viscosity of foam increasing initially with time as a result of syneresis followed by a decrease at longer times due to coarsening of bubble size. The presence of emulsion droplets decreased foam stability.

1. Introduction

Aerated food products are very popular. Foaming has become one of the fastest growing food processing operations for the development of new innovative products. Air is incorporated in the form of fine bubbles in order to render texture and mouthfeel to these products. Aeration can also help in mastication and enhance flavor delivery. The most commonly used aerated dairy products are ice cream, whipped cream and mousses. Whipped cream, dairy desserts, milkshakes, beer, sparkling wine, carbonated soft drinks are examples of some of liquid aerated products. Aeration is also employed in several other food products such as beer, sparkling wine, bread, cakes, breakfast cereals, meringue, aerated chocolate bars, vegetable paste foams, sorbet and aerated meat foams.

The incorporated bubbles are usually stabilized by proteins and other food emulsifiers which, being surface active, adsorb onto the bubble surface and prevent coarsening due to coalescence by modifying the interparticle forces as well as by providing interfacial rheological properties. In liquid products, air incorporation results in an air–liquid dispersion in which the air bubbles cream (due to density difference) to the top to form a foam layer. The texture and shelf life of the foam layer depends on the amount of liquid retained by the foam which, in turn, is determined by syneresis. Excellent reviews on creation and characterization of aerated food products (Campbell and Mougeot, 1999), and foam stability (Murray and Ettelaie, 2004) can be found. Bubble size (Djelveh and Gros, 1995) and residence time distribution (Thakur et al., 2003) have been correlated to number of paddles, shear rate and gas–liquid ratio in a laboratory scale scraped surface mixer. Unlike pure protein stabilized foams, aerated cheese product made in a continuous scraped surface heat exchanger (Vial et al., 2006a) exhibited minimum stability near p*I* of casein presumably due to inferior viscoelastic properties of the continuous phase at this pH. A minimum solids content in the cheese formulation (Vial et al., 2006a) was found to be necessary to prevent creaming of incorporated air bubbles. Foamability and foam stability of aerated cheese were found to be enhanced by the addition of whey protein concentrate, high melting point fat fraction and phospholipids whereas mono and triglycerides had a detrimental effect (Vial et al., 2006b).

Breakup of an air bubble due to the application of shear requires the application of a critical external shear force to counteract the surface tension forces. Addition of proteins and emulsifiers result in a decrease in the surface tension and therefore makes it easier for bubble breakup. Relative motion between two bubbles induced by the application of shear, results in their collision which may lead to coalescence. Every collision does not result in coalescence because of the repulsive colloidal interactions between bubbles. These collidal interactions are influenced by the adsorbed protein/emulsifier layer which imparts electrostatic and steric

* Corresponding author. Tel.: +1 765 494 1199; fax: +1 765 496 1115.
E-mail address: narsimha@purdue.edu (G. Narsimhan).

0260-8774/$ - see front matter © 2008 Elsevier Ltd. All rights reserved.
doi:10.1016/j.jfoodeng.2008.03.003

repulsive interactions that are dependent on the ionic strength of the continuous phase, the layer thickness, molecular weight, conformation of protein and interaction of protein with the continuous medium (protein hydrophobicity) (Narsimhan, 1992, 2005b). In addition, gums in the continuous phase provide interaction force between colliding bubbles resulting from the depletion of macromolecules/particles in the region between the bubbles (Narsimhan, 1992). The net effect of these interactions on the collision efficiency can be expressed in terms of stability ratio (Hiemenz and Rajagopalan, 1997).

Air bubbles in the foam layer that is formed by creaming are distorted in the form of polyhedra and are separated by thin films. Three adjacent thin films intersect in a Plateau border and the continuous phase is interconnected through a network of Plateau borders (Bikerman, 1973). The stability of foam is intricately related to syneresis that occurs invariably in foam because of gravity and capillary forces. As the liquid in the Plateau border drains due to gravity through a Plateau border network (Desai and Kumar, 1982; Leonard and Lemlich, 1965; Narsimhan and Ruckenstein, 1995), the top of the foam becomes drier. This Plateau border suction also leads to drainage of liquid from thin films to the neighboring Plateau border. In protein stabilized foams, this is counteracted by disjoining pressure caused by van der Waals, electrostatic and steric interactions between two approaching faces of a draining film (Ivanov, 1988). The film may also rupture due to the growth of imposed thermal and mechanical perturbations (Ivanov and Dimitrov, 1974; Narsimhan, 2005a) thus leading to coalescence of neighboring gas bubbles. Previous studies on syneresis have investigated the effect of different variables on the accumulation of liquid layer (Desai and Kumar, 1983; Germick et al., 1994; Sita Ram Sarma and Khilar, 1988, 1990; Sita Ram Sarma et al., 1988) and evolution of liquid holdup profile (Saint-Jalmes and Langevin, 2002; Wang and Narsimhan, 2004, 2006) within the foam.

Only limited empirical studies have been made recently (Vial et al., 2006a, b) for the production of aerated food using continuous shearing. Delineation of different mechanisms of stabilization of air–liquid dispersion as well as foam by macromolecules, emulsion droplets and hydrophobic/hydrophilic particles is necessary for a rational choice of ingredients and operating conditions for such a process. In this paper, the effects of different operating conditions such as rotational speed, air–liquid ratio and process parameters such as gum concentrations, pH, ionic strength and temperature on the bubble size, apparent viscosity and syneresis of foam produced in a continuous shearing apparatus is presented.

2. Materials and methods

2.1. Sample procedure

The following materials were used for the research: casein sodium salt from bovine milk (Sigma Chemical Co., St. Louis, MO), xanthan gum (Sigma Chemical Co., St. Louis, MO), sodium phosphate monobasic anhydrous NaH_2PO_4 (Sigma Chemical Co., St. Louis, MO), and sodium phosphate dibasic anhydrous Na_2HPO_4 (Mallinckrodt Chemical Inc, Paris, KY).

General Procedure: 2% (w/w) sodium caseinate protein solution buffered using sodium phosphate (pH 7.0 and ionic strength 0.01 M) was transferred by a peristaltic pump (MasterFlex L/S, Colepalmer Instrument Company) from a beaker into the shear mixer at a controlled inlet flow rate. Air from compressed air line at a controlled pressure (using a pressure regulator) was introduced into the shear mixer at a desired flow rate (measured using a flow meter). The inner cylinder of the shear mixer was rotated at a fixed rpm using a dc motor with a speed control. The gas–liquid dispersion formed in the shear mixer was collected in a plastic cup for foam volume fraction measurement. The gas bubbles of the dispersion creamed rapidly to form a foam layer at the top and a liquid layer at the bottom. Some foam was transferred to a glass slide and examined using a light microscope at a magnification of around 80. Another sample was collected in a glass tube with an inner diameter of 13 mm and a height of 20 mm for magnetic resonance imaging (MRI) analysis.

2.2. Continuous foaming process

A lab-scale shear mixer apparatus (see Fig. 1) consisted of a double-concentric cylinders (diameter of 50 mm, length of 300 mm and a gap of 1 mm) where the outer cylinder was stationary and the inner cylinder was rotating, a peristaltic pump (to transfer the protein solution/emulsion at the desired flow rate), a flowmeter to control the air flow rate, and a motor to adjust the mixing speed of the inner cylinder. The gas–liquid dispersion was collected from the outlet in a plastic cup, which was analyzed for foam characterizations.

2.3. Foam volume fraction

The gas–liquid dispersion from the continuous shear mixer was collected in a plastic cup. Heights of the foam and liquid were measured as a function of time. The volumes of foam and liquid were determined from their heights using the geometry of the cup. Foam volume fraction was referred to as the ratio of foam volume (V_{foam}) to total volume ($V_{liquid} + V_{foam}$).

2.4. Foam wetness

In addition, the amount of liquid entrained inside the foam layer ($V_{liq,foam}$) was measured by subtracting the total weight of gas–liquid dispersion collected (W_{tot}) from the weight of liquid on the bottom liquid layer (W_{liquid}). The foam wetness was defined as the amount of liquid inside the foam layer divided by the volume of foam, i.e.

$$\text{Foam wetness} = \frac{V_{liq,foam}}{V_{foam}}$$

2.5. Liquid fraction in foam (liquid holdup)

The variation of liquid holdup with height was measured using magnetic resonance imaging (MRI). This technique has been used previously (Wang and Narsimhan, 2004) to study the amount of liquid entrained in the foam (liquid holdup). The sample cell with an inner diameter of 13 mm and height of 20 mm was inserted into a large glass tube. The glass tube was then inserted into a 20 MHz

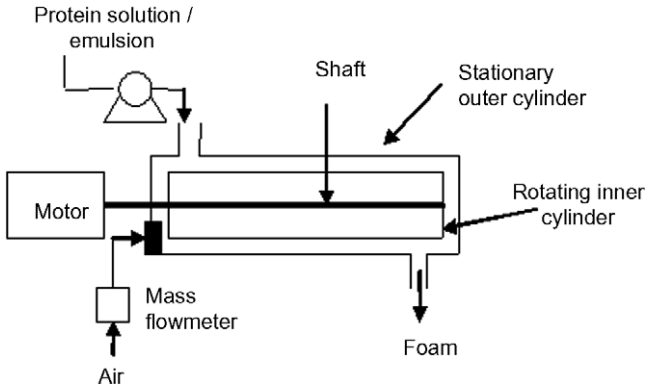

Fig. 1. Schematic of a double-concentric cylinder shear mixing apparatus.

MARAN Ultra Magnetic Resonance imaging spectrometer (Resonance Instruments Ltd.).

The sample was scanned to produce ^{1}H spectra at 15 MHz at 2, 5, 10, 15 and 20 min after the foam was collected into a sample tube. Only one scan could be performed for each profile with a signal to noise ratio of about 6% because of time constraints for transient measurements. The interval between the 90° and 180° pulses for the MRI was 3 ms, and pre-delay between successive signal acquisitions was 15 s.

Liquid fraction in foam was obtained from the MRI profile. The liquid holdup was calculated by normalizing the MRI signal with that for pure water. The details of this method are given elsewhere (Wang and Narsimhan, 2004). The integral of liquid holdup over the height of the foam layer gave the liquid in foam and the integral over the whole tube gave the total liquid. The liquid fraction in foam was obtained by dividing the liquid in foam by the total liquid.

2.6. Apparent viscosity index

The apparent viscosity of the foam was characterized using a Brookfield viscometer (Brookfield Engineering Labs, Inc., Stoughton, MA) with a stainless steel T-spindle (Brookfield #91, 48.1 mm wide and 0.73 mm in diameter). The T-spindle was lowered to exactly the middle of the foam and the rotational speed of spindle was increased stepwise from 0.5 to 60 rotations per minute, depending on the wetness of foam. These measurements were made at 2, 5, 10, 20 min after the foam was collected into a plastic cup. Three replicates were conducted for each set of experiment.

Since constant shear rate cannot be maintained in a T-spindle, these measurements do not yield "true apparent viscosity" of foam. Consequently, the "apparent viscosity" readings obtained from the instrument are a measure of torque divided by angular velocity, with a geometric factor. These readings were then converted to "apparent viscosity index", using,

$$\eta_{app}\ \text{index} = \frac{\eta_{app}\ \text{foam}}{\eta_{app}\ \text{glycerin}} \cdot 1485cP \quad (1)$$

where η_{app} foam and η_{app} glycerine are the apparent viscosities of foam and glycerin measured using a T-spindle in Brookfield viscometer, respectively, at certain spindle speed, 1485*cP* is the viscosity of glycerin (www.reference.com/browse/wiki/Viscosity).

2.7. Bubble size

A small sample of foam was placed in a glass slide under a light microscope (Spencer) with an amplification of 80. Photographs were taken using Polaroid instant pack films. Then the photographs were analyzed using Scion Image Analysis software to obtain the mean bubble size as well as bubble size distribution. About 100–300 bubbles were counted for each sample.

2.8. Zeta potential

Electrophoretic mobility measurements of air bubbles with adsorbed protein layer were made with Zetameter 3.0 particle electrophoresis unit. The air–liquid dispersion that was collected from the system was allowed to separate into foam and dispersion layers. The air bubbles were transferred from the dispersion layer into the sample cell of the Zetameter. The movement of the air bubbles due to an applied electric field was monitored using dark-field microscope in order to obtain the electrophoretic mobility. The zeta potential of the air bubbles was inferred from the analysis of movement of bubbles under the influence of electric field and the viscous resistance to movement in a power law fluid. The details of this analysis is given elsewhere (Indrawati and Narsimhan, in preparation). The inference of zeta potential requires the bubble size and the power law rheological parameters of xanthan gum solutions. Bubble size of dispersion was determined using the methods described above. The power law parameters were inferred from the shear stress versus shear rate measurements using capillary rheometer RH 2000 (Bohlin instruments, Gloucestershire, England) rheometer.

2.9. Emulsion preparation

An aqueous solution was prepared by mixing sodium caseinate (2% w/w), xanthan gum (0.2% w/w), vegetable oil (10% by volume) and phosphate buffer (pH 7 and ionic strength of 0.01 M). The solution was premixed using a high-shear vortex (VirTishear, The Virtis Co., Gardiner, NY) for 2 min, and then was homogenized using a two-stage high pressure valve homogenizer (15MR, APV Gaulin Inc.) to reduce the emulsion droplet size at homogenizer pressure of 4000 psi at first stage and 500 psi at the second stage.

3. Results and discussion

All experiments were carried out using a double-concentric cylinder shear mixing apparatus, as shown in Fig. 1. Two different concentrations of xanthan gum were used to increase the viscosity of the continuous phase: 0.1 and 0.2% (w/w). The protein solution was prepared by mixing 2% sodium caseinate with the addition of xanthan gum (0.1 and 0.2% w/w). The solution was then transferred into the shear mixing apparatus at flow rate in the range of 5–10 ml/s, while, air was also injected to the system at a flow rate in the range of 1.7–5 ml/s to produce a dispersion of different air liquid ratios. The mixing speed was varied in the range of 900–1800 rpm. The air–liquid dispersion was collected in a plastic cup for characterization.

3.1. Effect of mixing speed

The initial average bubble size of foams at different mixing speeds (bubble size measurement was made immediately after gas–liquid dispersion was collected) for two different xanthan gum concentrations is shown in Fig. 2. As expected, bubble size decreased as mixing speed increased for both xanthan gum concen-

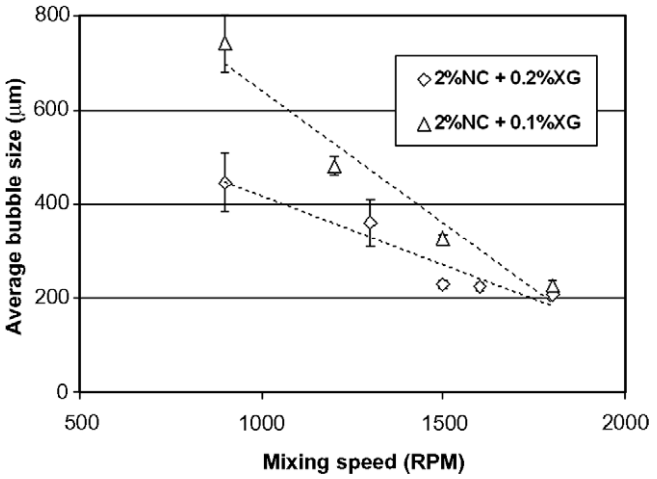

Fig. 2. The average bubble size as a function of mixing speed for 2% sodium caseinate with the addition of 0.1% and 0.2% of xanthan gum at pH 7 and ionic strength 0.01 M. The liquid flow rate is 5 ml/s. The air flow rate is 5 ml/s. The air–liquid ratio is 1:1.

trations. The decrease in bubble size is due to more bubble breakup as a result of higher shear stress at higher mixing speed. Same trend was observed by other researches (Djelveh and Gros, 1995; Thakur et al., 2003; Vial et al., 2006a). In addition, smaller bubbles were observed for higher gum concentration of 0.2%, which is consistent with earlier observations in a stator–rotor mixing systems (Belerin et al., 2007; Hanselmann and Windhab, 1999). This is believed to be due to the combined effects of: (a) more bubble breakage as a result of higher applied shear stress and (b) lower bubble coalescence due to slower liquid drainage between colliding bubbles resulting from higher viscosity.

It is also instructive to plot the bubble size at different rotational speeds in terms of Weber number, a dimensionless number which is the ratio of shear stress and the capillary pressure acting on the bubble. Choosing the characteristic length as the gap h between the rotor and the stator, the Weber number can be defined as,

$$We = \frac{K(ND)^n}{h^{n-1}\gamma} \tag{2}$$

where K and n are the consistency index and flow behavior index, respectively, of xanthan gum solution, D is the rotor diameter and γ is the surface tension. The plot of d_{32} versus We for two different xanthan gum concentrations and different air–liquid ratio are shown in Fig. 3a and b, respectively. It is interesting to note that the plots for two different xanthan gum concentrations collapse into a single curve. Also, the difference in d_{32} for different air–liquid ratios is found to be statistically insignificant except at large Weber number.

The foam volume fraction decreased somewhat from 90% to 80% as the mixing speed decreased from 1800 to 1200 rpm (Fig. 4). However, further decrease in the speed to 900 rpm resulted in a large decrease in % foam (60%). At higher mixing speed, the bubble size was smaller because of higher shear which led to more gas–liquid surface area, more liquid entrainment and hence higher foam volume.

3.2. Evolution of liquid holdup profile

The typical liquid holdup profiles measured by magnetic resonance imaging (MRI) in the foam that was produced at a mixing speed of 1800 rpm at different times are shown in Fig. 5. The profile shows a liquid region of holdup equal to unity and a foam region of much smaller liquid holdup with a sharp transition due to foam–liquid interface. Because of accumulation of liquid at the

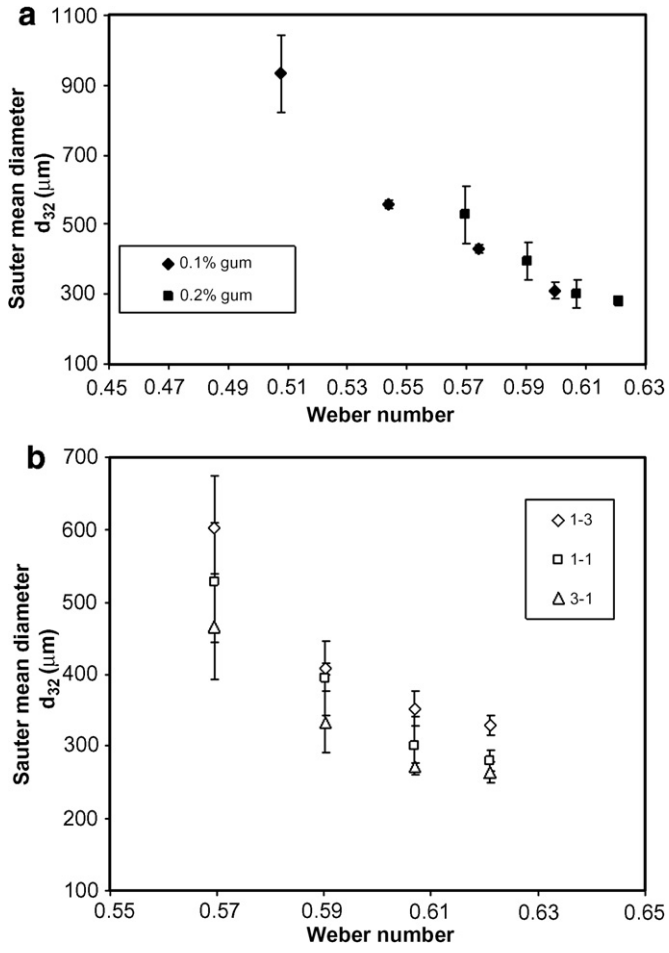

Fig. 3. (a) Sauter mean bubble diameter versus Weber number for different gum concentrations. The other conditions are the same as given in Fig. 2. (b) Sauter mean bubble diameter versus Weber number for different air–liquid ratios at 0.2% xanthan gum concentration. The other conditions are the same as given in Fig. 2. For air–liquid ratio of 1:1, the liquid and air flow rates are equal at 5 ml/s. For air–liquid ratio of 3:1, the air flow rate is 5 ml/s and the liquid flow rate is 1.7 ml/s. For air–liquid ratio of 1:3, the air flow rate is 1.7 ml/s and the liquid flow rate is 5 ml/s.

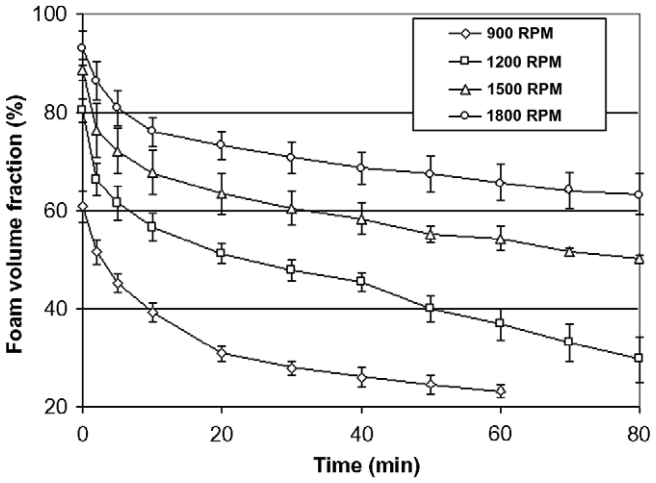

Fig. 4. Foam volume fraction as a function of mixing speed for 2% sodium caseinate solution with 0.2% xanthan gum for air–liquid ratio of 1:1.

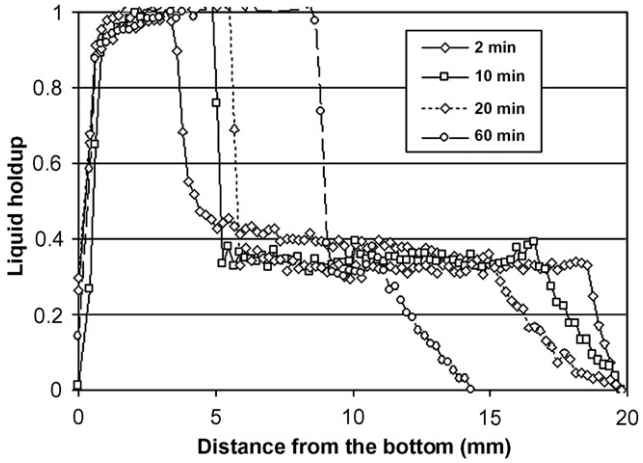

Fig. 5. The MRI profiles for 2% sodium caseinate solutions with addition of 0.2% xanthan gum at a mixing speed of 1800 rpm as a function of time. Other conditions are the same as given in Fig. 2.

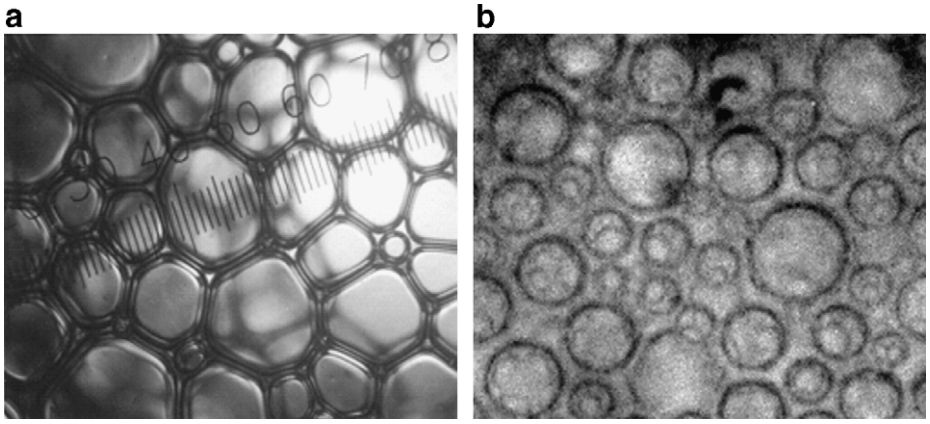

Fig. 6. Photographs of bubbles in: (a) foam layer and (b) cream layer.

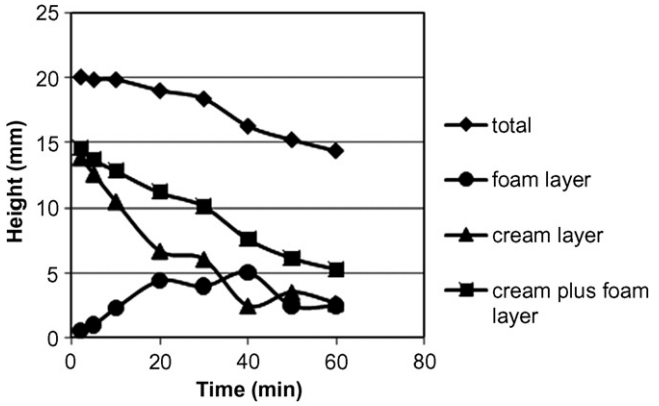

Fig. 7. Variation of total, foam plus cream layer, cream layer and foam heights with time for foam formed with 2% sodium caseinate solutions with addition of 0.2% xanthan gum at a mixing speed of 1800 rpm. Other conditions are the same as given in Fig. 2.

bottom as a result of syneresis, the amount of liquid phase increases with time. For example, the height of bottom liquid phase increased from 4 mm at 2 min to 9.0 mm at 60 min. It is interesting to note that the foam region consists of a region of constant liquid holdup (greater than 0.26, value for close packed spheres) above which is the second foam layer.[1] Typical photographs of bubbles in the foam and cream layers are shown in Fig. 6a and b, respectively. It is to be noted that the bubbles are distorted in the form of polyhedra in the foam layer whereas they are spherical in the cream layer. It is believed that the region of constant liquid holdup corresponds to a cream layer[2] of concentrated air–liquid dispersion in which the air bubbles are not distorted since the liquid holdup in this layer is greater than 0.26, value for close packed spheres. The variation of total height of mixture, foam plus cream layer, foam layer and cream layer with time is shown for 0.2% xanthan gum solution in Fig. 7. Because of syneresis, the total height of cream layer decreases and the height of foam layer increases up to 40 min. At longer times, however, the total height of the foam layer starts decreasing because of the predominant effect of bubble coalescence at the top. Also, the liquid holdup within the cream layer was found to decrease linearly with height, this decrease being more pronounced at 2 min than at longer times. In addition, the liquid holdup profile within the foam region became less steep as a result of syneresis. The decrease in the total height with time can be attributed to bubble coalescence at the top.

3.3. Effect of xanthan gum concentration

The effect of xanthan gum concentration on evolution of MRI profile is shown in Fig. 8. The evolution of total height, heights of cream and foam layer for two gum concentrations is shown in Fig. 9.The amount of foam (cream plus foam layer) produced was much higher at 0.2% xanthan gum concentration compared to that at 0.1% (Fig. 9). Also, most of the foam consisted of cream layer at 2 min. for 0.2% gum solution whereas the cream layer fraction was smaller for 0.1% gum solution (see Figs. 8 and 9). This is consistent with our earlier observations for foams stabilized by β lactoglobulin (Wang and Narsimhan, 2006). Foam produced with 0.2% xanthan gum was found to be very stable as indicated by much slower rate of decrease in total height (Fig. 9). On the other hand, significant bubble coalescence at the top of the foam resulted in a much faster rate of decrease of total height for foam produced with 0.1% xanthan gum (Fig. 9). Similar effects of gum concentration on drainage and collapse of sodium caseinate stabilized foams have been reported earlier (Wang and Narsimhan, 2004). Carp

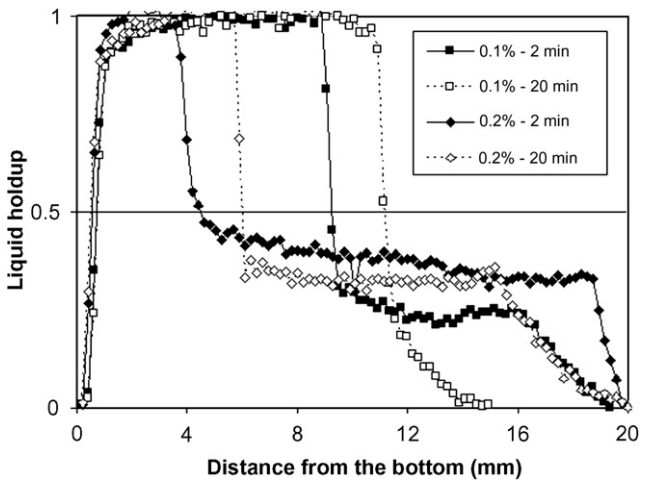

Fig. 8. The MRI profiles for 2% sodium caseinate solutions for different xanthan gum concentrations as a function of time. Other conditions are the same as given in Fig. 2.

[1] The liquid volume fraction in the foam layer is less than 0.26 (fraction corresponding to close packed spheres). As a result, the bubbles in the foam layer are distorted in the form of polyhedra.

[2] The liquid volume fraction in the cream layer is greater than 0.26. As a result, the bubbles in the cream layer are not distorted. Therefore, the cream layer can be considered as a layer of concentrated air–liquid dispersion.

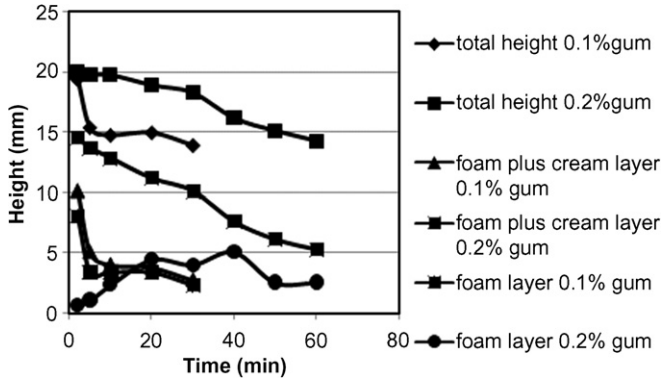

Fig. 9. Variation of total, foam plus cream layer, cream layer and foam heights with time for foam formed with 2% sodium caseinate solutions at a mixing speed of 1800 rpm for two different xanthan gum concentrations. Other conditions are the same as given in Fig. 2.

et al. (2001) reported that addition of xanthan in soy protein isolates caused reduced rates of drainage and foam height collapse. Another study showed that addition of xanthan gum in whey protein isolate increased stability to 15 times that without gum (Mott et al., 1999).

3.4. Effect of air–liquid ratio

The effect of air–liquid ratio on evolution of MRI profile and foam height are shown in Figs. 10 and 11, respectively. As expected, the amount cream plus foam layer was higher at higher air–liquid ratio (Fig. 10). As a result, syneresis was faster at higher air–liquid ratio thus resulting in a much larger increase in the amount of liquid at the bottom. Also, the foam that was produced at higher air volume fraction was less stable, i.e. the height of the foam layer decreased faster (Fig. 11). Wetter foam was less stable because of faster syneresis consistent with the observations of Sita Ram Sarma and Khilar (1988).

3.5. Apparent viscosity

The apparent viscosity index of foam produced at different mixing speeds as a function of time at a constant shear rate corresponding to spindle speed of 5 rpm is shown in Fig. 12. Foams

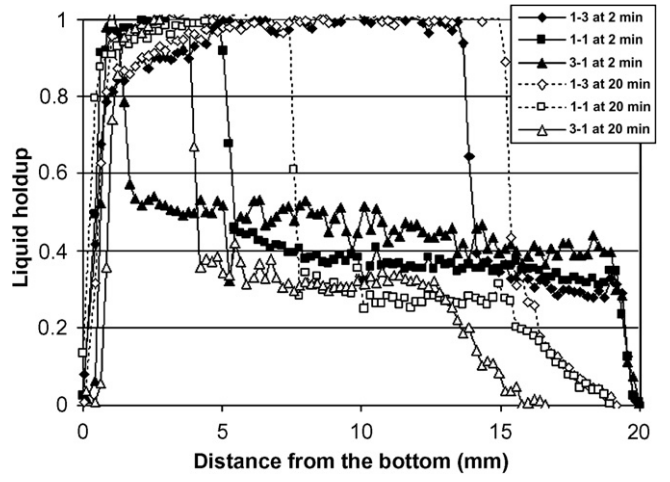

Fig. 10. The MRI profiles for 2% sodium caseinate solutions with addition of 0.2% xanthan gum at different air–liquid ratios as a function of time. Other conditions are the same as given in Fig. 2.

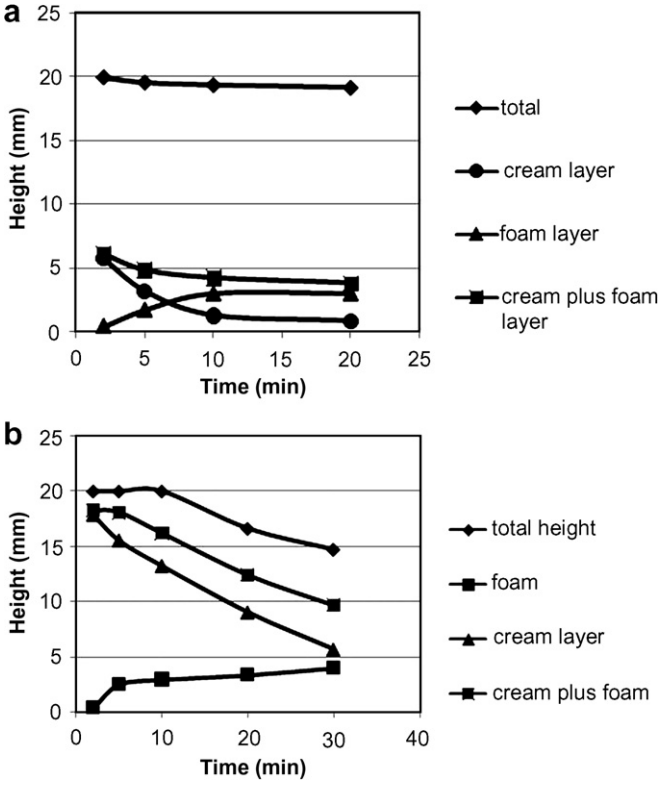

Fig. 11. Variation of total, foam plus cream layer, cream layer and foam heights with time for foam formed with 2% sodium caseinate solutions at a mixing speed of 1800 rpm for different air–liquid ratios: (a) 0.25 (b) 0.75.

produced at higher mixing speed exhibited lower apparent viscosity due to more liquid entrainment in the foam layer (wetter foam). Drainage and bubble coalescence are the important factors that determine the change in the apparent viscosity. As a result of liquid drainage, the foam becomes drier which leads to an increase in its apparent viscosity. However, because of bubble coalescence, the average bubble size increases (see inset in Fig. 12). This increase in bubble size leads to lower apparent viscosity of the foam. At smaller times, the former effect predominates whereas the latter

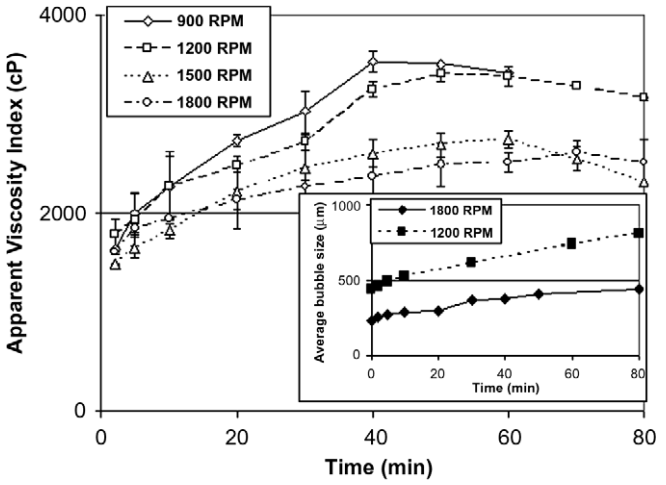

Fig. 12. Apparent viscosity as a function of time for foams formed at different mixing speeds for 2% sodium caseinate solution with 0.2% xanthan gum. Inset: bubble size as a function of time for mixing speed of 900 and 1800 rpm. Other conditions are the same as given in Fig. 2.

Table 1
Zeta potential (ZP) of bubbles with adsorbed protein layer

pH	Ionic strength (M)	Temperature (°C)	Voltage (V)	Conductance (Ω/cm)	EM (μ/s cm/V)	ZP (mV)
7	0.01	21	100	1300 ± 10	−0.212 ± 0.02	−102.6 ± 1.3
	0.01	60	100	1380 ± 56	−0.161 ± 0.01	−78.3 ± 2.8
	0.02	21	100	1710 ± 103	−0.203 ± 0.01	−80.2 ± 1.1
	0.05	21	75	322 0 ± 14	−0.161 ± 0.02	−42.8 ± 2.5
	0.1	21	50	5310 ± 183	−0.085 ± 0.01	−9.4 ± 1.2
6	0.01	21	100	1630 ± 20	−0.128 ± 0.01	−55.9 ± 1.8
9	0.01	21	100	1183 ± 30	−0.232 ± 0.01	−118.2 ± 2.7

The foams were formed with 2% sodium caseinate with the addition of 0.1% of xanthan gum. The liquid and air flow rates in the shear apparatus were equal at 5 ml/s with the air–liquid ratio of 1:1.

effect becomes important at longer times thus leading to a maximum in apparent viscosity. All foams were shear thinning in that the apparent viscosity decreased with rpm of the spindle (results not shown).

At lower air–liquid ratio, the foam is wetter and therefore the liquid drainage is faster which results in a faster increase in apparent viscosity and a faster decrease in foam wetness (results not shown). This increase in liquid drainage can also be attributed to larger bubble size at lower air–liquid ratio (see Table 2). However, as explained earlier, there is a maximum in apparent viscosity because of predominant effect of bubble coalescence at larger times. Interestingly, the foam at highest air–liquid ratio of 3–1 (driest foam) does not exhibit any significant change in apparent viscosity as a result of negligible liquid drainage (negligible change in foam wetness).

3.6. Effect of oil

Comparison of evolution of foam volume fraction for foams formed with and without oil emulsion drops (results not shown) indicates that the presence of oil droplets has a destabilizing effect on foam as can be seen from an increase in the decay rate for foams in the presence of oil droplets.

3.7. Effect of ionic strength

The effect of ionic strength on the evolution of foam volume fraction is shown in Fig. 13. The initial amount of foam formed was highest for lowest ionic strength (0.01 M) and decreased as ionic strength increased. This decrease was significant only for ionic strength of 0.1 M. The foam was more stable at lower ionic strengths as indicated by slower rate of decrease in foam volume fraction. Higher stability at lower ionic strength can be attributed to larger electrostatic repulsive interactions as evidenced by higher zeta potential values (see Table 1). This is consistent with the reported effect of ionic strength on zeta potential of bubbles stabilized by proteins (Phianmongkhol and Varley, 2003). The zeta potential values of −42.8 and −80.3 mV (Table 1) at ionic strengths of 0.05 and 0.01 M, respectively, compare well with the values in

Table 2
Bubble size at initial time for foams formed with 2% sodium caseinate with the addition of 0.1% of xanthan gum

pH	Ionic strength (M)	Temperature (°C)	Air–liquid ratio	d_{32} (μm)	d_{av} (μm)
6	0.01	21	1–1	324 ± 13	268 ± 19
7	0.01	21	1–1	280 ± 23	216 ± 11
7	0.01	21	1–3	376 ± 30	274 ± 11
7	0.01	21	3–1	243 ± 12	195 ± 15
7	0.01	60	1–1	305 ± 10	241 ± 8
9	0.01	21	1–1	256 ± 36	204 ± 26

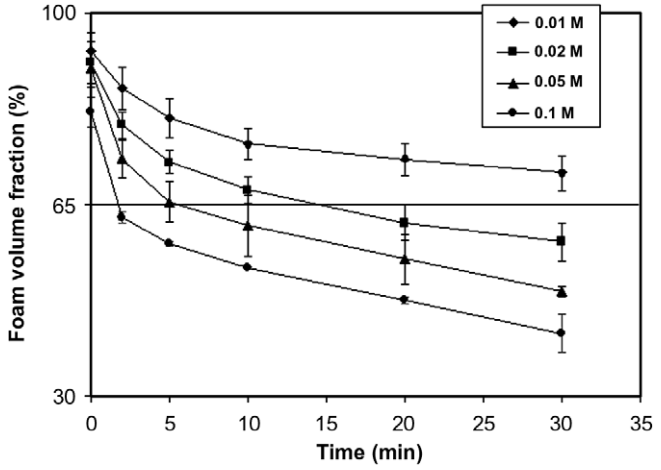

Fig. 13. Foam volume fraction as a function of ionic strength at rotational speed of 1800 rpm for 2% sodium caseinate solution with 0.2% xanthan gum at pH 7. Other conditions are the same as given in Fig. 2.

the range of −30 to −50 mV reported (Phianmongkhol and Varley, 2003) for bovine serum albumin and lysozyme in the concentration range of 0.1–0.8 mg/ml at an ionic strength of 0.005 M at pH 7. It is believed that the values reported here are larger than the literature values because of much higher protein concentration (20 mg/ml) employed. The effect of ionic strength on the evolution of total height, foam plus cream layers and liquid layer are shown in Fig. 14. The foam was quite stable at ionic strength of 0.01 M compared to 0.02 M as indicated by much smaller change in total height (Fig. 14). Order of magnitude estimates of double layer repulsive disjoining pressure for a film of 10 nm thickness at two ionic strengths indicate a decrease in disjoining pressure from about 4×10^4 Pa at ionic strength of 0.01 M to 10^4 Pa at ionic strength of 0.02 M. However, at ionic strength of 0.1 M, the foam was quite unstable as indicated by the movement of the top position of foam with time (not shown). This is understandable since the zeta potential at this ionic strength has dropped to −9.4 mV compared to a value of −102.6 mV at 0.01 M (Table 1) thus resulting in negligible double layer repulsive disjoining pressure. In fact, the height of foam layer increased with time as a result of creaming up to 5 min followed by a decrease at longer times due to foam collapse. In addition, syneresis was much faster at ionic strength of 0.02 M as evidenced by a much faster decrease in foam plus cream layers (Fig. 14). This can be attributed to larger bubble size at higher ionic strength (see Fig. 15). It has been shown that larger bubble size leads to faster Plateau border drainage (Wang and Narsimhan, 2004). In addition, higher ionic strength will result in lower electrostatic repulsive interaction between the two faces of thin film and consequently will lead to faster thin film drainage. Apparent viscosity was highest for foams formed at an ionic strength of 0.1 M as a result of faster liquid drainage. The apparent viscosity

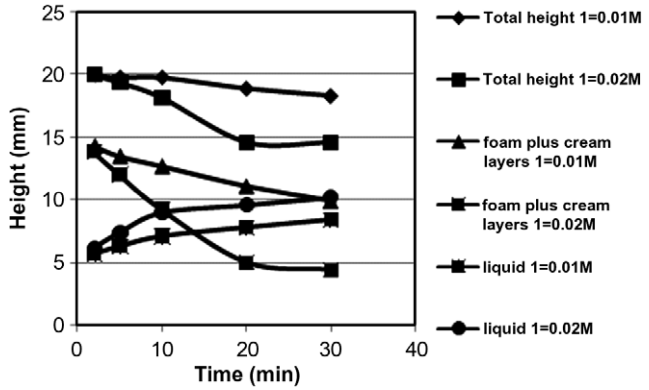

Fig. 14. Variation of total, foam plus cream layer, cream layer and foam heights with time for foam formed with 2% sodium caseinate solutions at a mixing speed of 1800 rpm for different ionic strengths. Other conditions are the same as given in Fig. 2.

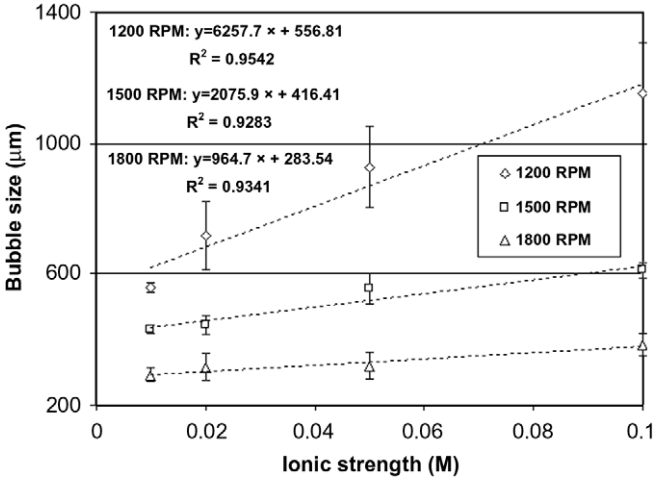

Fig. 15. The sauter mean diameters as a function of rotational speed for foam formed at different ionic strengths for 2% sodium caseinate solution with 0.2% xanthan gum at pH 7.

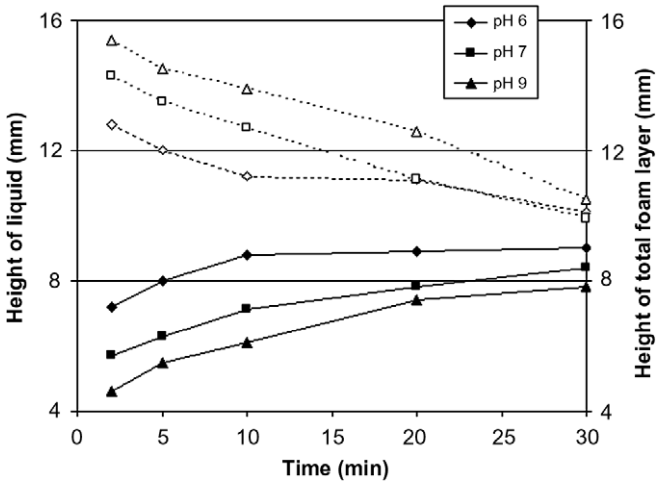

Fig. 16. The height of liquid layer (solid lines) and combined height of cream and foam layers (dashed lines) as a function of time for foam formed at different pH for 2% sodium caseinate solution with 0.2% xanthan gum at ionic strength of 0.01 M.

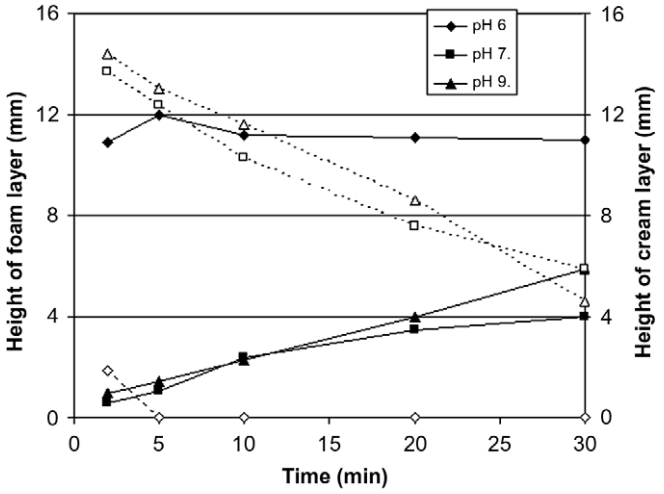

Fig. 17. The height of foam layer (solid lines) and height of cream layer (dashed lines) as a function of time for foam formed at different pH for 2% sodium caseinate solution with 0.2% xanthan gum at ionic strength of 0.01 M.

decreased with ionic strength being lowest at ionic strength of 0.01 M. The variation of Sauter mean bubble diameter with ionic strength for foams that were produced at different rotational speed of the rotor is shown in Fig. 15. The bubble size increased with ionic strength this increase being more pronounced at lower rotational speeds. This increase in bubble size with ionic strength is due to increased bubble coalescence rates during foam formation at higher ionic strength as a result of lower electrostatic repulsion between colliding bubbles.

3.8. Effect of pH

It is interesting to note that sample at pH 7 and 9 consisted mainly of liquid and cream layers whereas the sample at pH 6 consisted mainly of liquid and foam layers. The amount of liquid in the foam layer at pH 6 was much lower than that at pH 7 and 9 (results not shown) with the corresponding liquid layer being more at pH 6. The syneresis behavior was found to be similar at pH 7 and 9 (the profiles not shown). The evolution of liquid height and combined height of dispersion and foam layers is shown in Fig. 16. As expected, the height of the liquid layer increases with time due to syneresis with the amount of liquid increasing from pH 9 to pH 6. The combined height of cream and foam layers was found to decrease with time due to the upward movement of foam–liquid interface. The position of the top of the foam remained the same except at times longer than 20 min thus indicating that the foam was quite stable. The evolution of heights of cream and foam layers is shown in Fig. 17. Interestingly, as pointed out above, the height of foam layer at pH 6 was much larger than those at pH 7 and 9. Faster syneresis at pH 6 can be attributed to larger bubble size. The foam layer increased with time at pH 7 and 9 as a result of creaming in the bottom cream layer which resulted in a decrease in its height. However, at pH 6, the height of the foam layer remained constant with time because of the absence of cream layer at longer times (see Fig. 16). The effect of pH on the bubble size is shown in Table 2. The average as well as sauter means bubble size was smaller at higher pH.

3.9. Effect of temperature

The effect of temperature on syneresis of foam is shown in Fig. 18. The initial amount of foam formed with 2% sodium caseinate was the same at 21 and 60 °C as can be seen from the inset

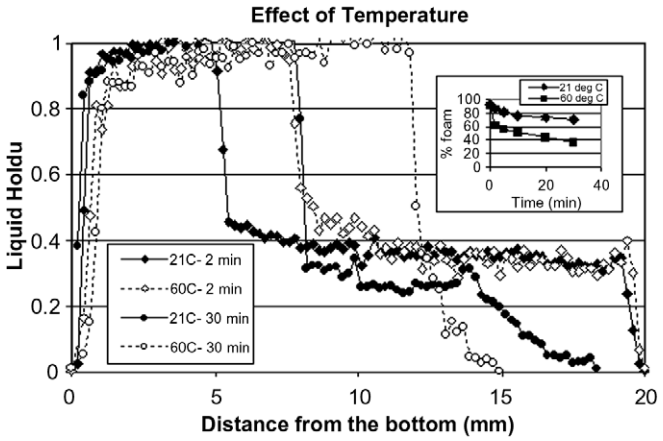

Fig. 18. The MRI profiles for different temperature of 2% sodium caseinate solutions with 0.2% xanthan gum at ionic strength of 0.01 M and rotational speed of 1800 rpm at 2 min after dispensation. Inset: % foam as a function of time for two temperatures.

in Fig. 18. Comparison of the liquid holdup profiles at 2 min for foams formed with 2% sodium caseinate at 21 °C and 60 °C indicate that more foam is retained at room temperature. Also, the initial average bubble size of foam formed at 60 °C was found to be larger (Table 2). More syneresis occurred for foams formed at 60 °C compared to that at 21 °C as evidenced by the liquid holdup profiles at 30 min shown in Fig. 18. This is consistent with the observations of Pradhan et al. (1990) and can be attributed to decrease in apparent viscosity at higher temperature. Model predictions for syneresis in a standing protein stabilized foam (Wang and Narsimhan, 2004, 2006) have demonstrated increased drainage at lower apparent viscosities. In addition, the drainage rate is also influenced by several other variables such as bubble size, surface tension and zeta potential. The foam volume fraction also decreased much faster for foams formed at 60 °C compared to that at 21 °C (see inset of Fig. 18). At 60 °C, most of the foam collapses as the position of the top of the foam moves from 20 to 15 mm (Fig. 18). On the other hand, the foam formed at 21 °C was more stable as the top of the foam moves from 20 to 18.3 mm (Fig. 18). The lower stability at 60 °C can be attributed not only to higher thermal perturbations and lower viscosity but also to smaller electrostatic repulsion (due to smaller zeta potentials as shown in Table 1).

4. Conclusions

A continuous shearing apparatus was employed to make foam stabilized by sodium caseinate. The air bubbles in the air–liquid mixture that was collected from the shearing apparatus creamed to the top to form a foam layer. As a result of syneresis in the foam layer, the volume of liquid at the bottom increased. The foam was characterized by the measurements of bubble size, apparent viscosity index and evolution of liquid holdup profile due to syneresis. The effects of air–liquid ratio, rotational speed of the rotor, xanthan gum concentration, pH, temperature and ionic strength on foam characteristics were investigated. Bubble size decreased with rotational speed of the rotor with this decrease being more pronounced at lower xanthan gum concentrations. Foam stability was enhanced at higher gum concentration. The foam volume fraction was higher at higher mixing speed as a result of higher entrainment of liquid due to larger air–liquid interfacial area. Bubble size at different gum concentrations correlate well with dimensionless Weber number. The effect of air–liquid ratio on the bubble size is not significant. Syneresis in the foam layer resulted in an increase in the amount of liquid at the bottom with time. Eventhough the air volume fraction in the dispersion was initially uniform, syneresis resulted in the formation of a drier foam layer at the top which increased in height with time. The syneresis was faster at higher ionic strengths. In addition, the total height of the foam layer decreased as a result of foam collapse, this decrease being more pronounced at higher ionic strengths. The amount of foam was higher at higher air–liquid ratio and the foam that was produced at higher air–liquid ratio was more stable. The apparent viscosity index increased with time due to syneresis followed by a decrease at longer times as a result of coarsening of bubble size caused by coalescence. Consequently, the apparent viscosity index was maximum at an optimum intermediate time. The apparent viscosity index was lower at higher rotational speed and higher for higher air–liquid ratios. The sauter mean bubble size increased with ionic strength this increase being more pronounced at lower rotational speeds. Foam that was produced at pH 6 was drier, with liquid holdup less than 0.26 (holdup for close packed spheres), than that produced at pH 7 and 9. The bubble size was smaller for higher pH. Syneresis behavior was similar at pH 7 and 9. The presence of emulsion droplets resulted in less foam and was found to have a destabilizing effect on foam stability. Eventhough the same amount of foam was formed at 21 and 60 °C, the foam formed at higher temperature had larger bubbles and exhibited faster syneresis. Foam formed at 60 °C was less stable as a result of higher thermal perturbations, smaller electrostatic repulsion and lower viscosity.

References

Belerin, C., Aymard, P., Ducept, F., Vaslin, S., Cuvelier, G., 2007. Effect of formulation and processing factors on the properties of liquid food foams. J. Food Eng. 78 (3), 802–809.
Bikerman, J.J., 1973. Foams. Springer, New York.
Campbell, G.M., Mougeot, E., 1999. Creation and characterization of aerated food products. Trends Food Sci. Technol. 10, 283–296.
Carp, D.J., Bartholomai, G.B., Relkin, G.B., Pilosof, A.M.R., 2001. Effect of denaturation on soy–protein–xanthan interactions: comparisons of a whipping-rheological and bubbling methods. Colloid Surf. B 21, 163–171.
Desai, D., Kumar, R., 1982. Flow through a Plateau border of cellular foam. Chem. Eng. Sci. 37 (9), 1361–1370.
Desai, D., Kumar, R., 1983. Liquid holdup in semi-batch cellular foams. Chem. Eng. Sci. 38 (9), 1525–1534.
Djelveh, G., Gros, J.B., 1995. Estimation of physical properties of foamed foods using energy dissipation in scraped-surface heat exchangers. J. Food Eng. 26, 45–56.
Germick, R.J., Rehill, A.S., Narsimhan, G., 1994. Experimental investigation of static drainage of protein stabilized foams – comparison with model. J. Food Eng. 23 (4), 555–578.
Hanselmann, W., Windhab, E., 1999. Flow characteristics and modelling of foam generation in a continuous rotor–stator mixer. J. Food Eng. 38, 393–405.
Hiemenz, P.C., Rajagopalan, R., 1997. Principles of Colloid and Surface Chemistry, third ed. Marcel Dekker, New York.
Indrawati, L., Narsimhan, G. (in preparation). Inference of zeta potential of protein stabilized air bubbles in a non-Newtonian power law fluid.
Ivanov, I.B., 1988. Thin Liquid Films: Fundamentals and Applications. Marcel Dekker.
Ivanov, I.B., Dimitrov, D.S., 1974. Hydrodynamics of thin liquid films effect of surface viscosity on thinning and rupture of foam films. Colloid Polym. Sci. 252 (11), 982–990.
Leonard, R.A., Lemlich, R., 1965. Study of interstitial liquid flow in foam. AIChE J. 11 (1), 18–29.
Mott, C.L., Hettiarachchy, N.S., Qi, M., 1999. Effect of xanthan gum on enhancing the foaming properties of whey protein isolate. J. Am. Oil Chem. Soc. 76 (11), 1383–1386.
Murray, B.S., Ettelaie, R., 2004. Foam stability: proteins and nanoparticles. Curr. Opin. Colloid Interf. Sci. 9, 314–320.
Narsimhan, G., 1992. Emulsions. In: Schwartzberg, H.G., Hartel, R.W. (Eds.), Physical Chemistry of Foods. Marcel Dekker, Inc., pp. 307–386.
Narsimhan, G., 2005a. Rupture of thin stagnant films on a solid surface due to random thermal and mechanical perturbations. J. Colloid Interf. Sci. 287, 624–633.
Narsimhan, G., 2005b. Surface phenomena. In: Barbosa-Canovas, G.V. (Ed.), Food Engineering. UNESCO Publishing, pp. 191–213.
Narsimhan, G., Ruckenstein, E. (1995). Structure, drainage and coalescence of foams and concentrated emulsions. In: Prudhomme, R.K., Khan, S.A. (Eds.), Foams: Theory, Measurements and Applications, pp. 99–187.

Phianmongkhol, A., Varley, J., 2003. Zeta potential measurement for air bubbles in protein solutions. J. Colloid Interf. Sci. 260 (2), 332–338.
Pradhan, M.S., Sita Ram Sarma, D.H.S., Khilar, K.C., 1990. Stability of aqueous foams with polymer additives: II. Effects of temperature. J. Colloid Interf. Sci. 139 (2), 519–526.
Saint-Jalmes, A., Langevin, D., 2002. Time evolution of aqueous foams: drainage and coarsening. J. Phys. Condens. Matter 14 (40 SPEC), 9397–9412 (Liquid State Theory, from White Dwarfs to Colloids).
Sita Ram Sarma, D.H.S., Khilar, K.C., 1988. Effects of initial gas volume fraction on stability of aqueous air foams. Ind. Eng. Chem. Res. 27 (5), 892–894.
Sita Ram Sarma, D.H.S., Khilar, K.C., 1990. Comments on effects of electrolyte on the drainage of aqueous foams. J. Colloid Interf. Sci. 137 (1), 300–303.
Sita Ram Sarma, D.H.S., Pandit, J., Khilar, K.C., 1988. Enhancement of stability of aqueous foams by addition of water-soluble polymers – measurements and analysis. J. Colloid Interf. Sci. 124 (1), 339–347.
Thakur, R.K., Vial, C., Djelvah, G., 2003. Influence of operating conditions and impeller design on the continuous manufacturing of food foams. J. Food Eng. 60, 9–20.
Vial, C., Thakur, R.K., Djelveh, G., Picgirard, L., 2006a. Continuous manufacturing of a light-textured foamed fresh cheese by dispersion of a gas phase. I. Influence of process parameters. J. Food Eng. 77 (1), 1–13.
Vial, C., Thakur, R.K., Quintans, A.P., Djelveh, G., Picgirard, L., 2006b. Continuous manufacturing of a light-textured foamed fresh cheese by dispersion of a gas phase. Part II. Influence of formulation. J. Food Eng. 77 (1), 14–26.
Wang, Z., Narsimhan, G., 2004. Evolution of liquid holdup profile in a standing protein stabilized foam. J. Colloid Interf. Sci. 280 (1), 224–233.
Wang, Z., Narsimhan, G., 2006. Model for Plateau border drainage of power law fluid with mobile interface and its application to foam drainage. J. Colloid Interf. Sci. 300 (1), 327–337.